Journal of Membrane Science 660 (2022) 120841

Contents lists available at ScienceDirect

Journal of Membrane Science

journal homepage: www.elsevier.com/locate/memsci

Mixed matrix membranes based on ionic liquids and porous organic polymers for selective CO_2 separation

Ana R. Nabais [a], Sadia Ahmed [b], Muhammad Younis [b], Jin-Xiu Zhou [c], João R. Pereira [e,f], Filomena Freitas [e,f], David Mecerreyes [c,d], João G. Crespo [a], Mu-Hua Huang [b,**], Luísa A. Neves [a,***], Liliana C. Tomé [a,c,*]

[a] LAQV-REQUIMTE, Department of Chemistry, NOVA School of Science and Technology, FCT NOVA, Universidade NOVA de Lisboa, 2829-516, Caparica, Portugal
[b] School of Materials Science and Engineering, Beijing Institute of Technology, No. 5, Zhongguancun South Street, Beijing, 100081, China
[c] POLYMAT, University of the Basque Country UPV/EHU, Avda. Tolosa 72, Donostia-San Sebastian, 20018, Gipuzkoa, Spain
[d] Ikerbasque, Basque Foundation for Science, 48013, Bilbao, Spain
[e] Associate Laboratory I4HB - Institute for Health and Bioeconomy, NOVA School of Science and Technology, Universidade NOVA de Lisboa, 2829-516, Caparica, Portugal
[f] UCIBIO – Applied Molecular Biosciences Unit, Department of Chemistry, NOVA School of Science and Technology, FCT NOVA, Universidade NOVA de Lisboa, 2829-516, Caparica, Portugal

ARTICLE INFO

Keywords:
Iongel
Porous organic polymers
Ionic liquids
Gas separation

ABSTRACT

The development of more efficient materials is a crucial step in the development of gas separation membranes. In this work, we combine ionic liquids (ILs) and porous organic polymers (POPs) for the first time to fabricate a new type of mixed matrix iongel membranes, which are entirely composed of organic materials. The new azo-POPs reported in this work were specifically designed due to their "CO_2-philic" feature to be incorporated in iongel materials. The membranes, comprising 80 wt% of [C_2mim][TFSI] IL and 20 wt% of poly(ethylene glycol) diacrylate (PEGDA) network, were prepared using a solvent-free UV curing method. The unique properties of azo-POPs within the iongel material resulted in the fabrication of dense and defect-free membranes with improved gas separation performances, in terms of both CO_2 permeability (62.3–90.6 barrer) and, CO_2/CH_4 (9.9–12.0), CO_2/H_2 (6.0–12.1) and CO_2/N_2 (16.8–53.1) ideal selectivities, with the latter revealing to be highly dependent on the morphological properties of the azo-POPs. Furthermore, iongel characterization in terms of morphology, chemical structure and thermal properties, confirmed the potential of the novel mixed matrix iongels for CO_2 separation processes.

1. Introduction

The growing interest in understanding the full potential of membranes has led this class of materials to be considered a promising technology in processes such as the removal of CO_2 from flue gas streams (CO_2/N_2), natural gas/biogas upgrading (CO_2/CH_4) and hydrogen purification (CO_2/H_2) [1–5]. Despite their unquestionable advantages, the use of membranes for the separation of industrial gas streams at a large scale still needs to overcome some challenges in order to become a competitive technology. In this context, the search and development of more efficient materials is a crucial step in the development of advanced membranes, capable of combining high permeability and selectivity for specific gases with good thermal/chemical resistance, suitable mechanical properties, and long-term stability [6].

Among the different materials studied throughout the years, ionic liquids (ILs) have established themselves as one of the most versatile class of materials. The easy design and functionalization and the remarkable gas solubility of ILs have been essential features in the growth of IL-based membranes, either through the preparation of supported ionic liquid membranes (SILMs) [7–10], combination of ILs with

* Corresponding author. LAQV-REQUIMTE, Department of Chemistry, NOVA School of Science and Technology, FCT NOVA, Universidade NOVA de Lisboa, 2829-516, Caparica, Portugal.
** Corresponding author.
*** Corresponding author.
E-mail addresses: mhhuang@bit.edu.cn (M.-H. Huang), lan11892@fct.unl.pt (L.A. Neves), liliana.tome@fct.unl.pt (L.C. Tomé).

https://doi.org/10.1016/j.memsci.2022.120841
Received 31 March 2022; Received in revised form 7 June 2022; Accepted 13 July 2022
Available online 30 July 2022

poly(ionic liquids) (PILs) [11–13] or through the development of iongels, also called ionogels, ion gels or ionic liquid gel membranes [14–17]. Iongels are soft solid materials composed of a dispersed IL phase, which is usually the predominant component, and a solid continuous phase to form a three-dimensional structure, preserving the main properties of ILs and enabling the preparation of membranes with high IL content (> 60 wt%) [18].

One simple and efficient way to prepare iongels is by single-pot UV-initiated polymerization of a polymer network in the presence of the desired IL. In a previous work, we demonstrated a fast and simple methodology to prepare cross-linked iongel membranes, based on poly (ethylene glycol) diacrylate (PEGDA) and imidazolium-based ILs with different anions, namely $[TFSI]^-$, $[FSI]^-$, $[C(CN)_3]^-$ and $[B(CN)_4]^-$ [19]. Self-standing iongel membranes were prepared containing up to 90 wt% IL and the influence of the IL content and anion structure on the thermal and mechanical stability, as well as on the CO_2 solubility of the iongels, was studied. Finally, looking at the overall performance of the prepared iongels, it was possible to conclude that, although the cyano-based iongels presented higher CO_2 loading capacities, the iongels containing the [C_2mim][TFSI] IL showed the best compromise between CO_2 solubility and thermal/mechanical properties [19]. The conclusions drawn from this motivated us to further improve the performance of these materials through the incorporation of a third component. In the context of iongels, works related with the study of the incorporation of porous materials in an iongel composed predominantly of ILs are just in infancy [20–24].

Metal Organic Frameworks (MOFs), zeolites and graphene oxide (GO), are among the available and known materials, that can be used as a third porous component in the so-called mixed matrix membranes (MMMs) [25–27]. Recently, new synthetic routes are following the development of versatile and all-organic materials such as porous organic polymers (POPs).

POPs are a class of porous materials known for their high surface area, tuneable chemical functionalities and outstanding physicochemical stability, that have been used in several applications, such as catalysis [28–30], optoelectronics [31–33], chemical sensors [34–36], gas adsorption [37–39] and gas separation [40]. However, the use of POPs in gas separation membranes, particularly in membranes based on ILs, is yet to be explored.

In particular, azo-linked POPs, containing azo functional groups (R–N═N-R'), have shown large potential towards CO_2 capture for several reasons: the "CO_2-philic" nature of these materials arising from the Lewis acid-base interactions between CO_2 and azo groups leads to high CO_2 uptake capacity/selectivity, up to 5.36 mmol g^{-1} for ALP-1 [41]; they are composed of light elements (usually H, B, N, C and O) and are lightweight materials, therefore their gravimetric CO_2 capture capacities tend to be high and their BET surface areas are comparable to other porous materials, ranging from 400 to 1235 m^2 g^{-1} [41,42]. Depending on the synthetic route, and due to their easy functionalization, it is possible to design azo-POP structures and tailor their properties towards a specific separation [42]. Moreover, azo-POPs have a higher stability due to the nature of their covalent bonds, when compared to MOFs, which are linked through coordination bonds [42].

Structurally different azo-POPs and their potential towards CO_2 capture has been assessed throughout the recent years. For instance, Lu et al. [43] reported a facile synthesis of two different azo-linked POFs (azo-POF-1 and azo-POF-2) with moderate BET surface areas (up to 712 m^2 g^{-1}), but good CO_2 uptakes (up to 131 mg g^{-1} at 273 K) were obtained. Interestingly, the authors discovered that the highest CO_2/N_2 selectivity was achieved for the azo-POF with the largest average pore width. This shows that different porosity parameters should also be considered when analysing the affinity of these materials towards specific gases [43]. A simple and efficient preparation method was also reported by Yang and co-workers [44], where azo-functionalized microporous organic polymers (azo-MOPs) were synthesized at room temperature with yields over 95%. The resultant azo-MOPs, with a BET surface area around 706 m^2 g^{-1}, showed good thermal stabilities and high adsorption capacity for CO_2 (up to 134.8 mg g^{-1}), once again unveiling the potential of these materials for gas separation applications [44]. More recently, He et al. [45] highlighted the CO_2-philic properties of azo-POPs, by preparing mixed matrix membranes based on low molecular weight polyethylene glycol (PEG) 400 and Pebax®1657 with azo-POPs. PEG 400 and azo-POPs were combined through hydrogen bonding to effectively separate CO_2 from N_2, by enhancing the CO_2 permeability, from 94 barrer achieved by the unfilled Pebax®1657 membrane to 392 barrer, at 1 bar and 30 °C for the membrane with 1 mg mL^{-1} azo-POP [45].

Bearing in mind the potential shown by azo-POPs and the easy preparation of iongels, this work aims at providing a new approach regarding the preparation of mixed matrix membranes, by a solvent-free method, where it is possible to combine a high amount of IL (80 wt%) with an entirely organic filler, specifically designed for CO_2 separation. This work focuses on three main objectives: (i) the use of an efficient synthetic pathway to prepare four different azo-POPs; (ii) the fabrication and characterization of new UV cross-linked iongel membranes combining a polymer network (poly(ethylene glycol) diacrylate, PEGDA), 80 wt% [C_2mim][TFSI] IL and four structurally different azo-POPs, using a straightforward solvent-free method; and (iii) understand how the azo-POP structures and their functional azo groups can impact CO_2 separation, which had only been explored through adsorption experiments or molecular simulation studies, so far. Besides the improvement in the separation performance of the iongels containing azo-POPs, it is expected that a high compatibility between all the materials can be achieved, due to the organic nature of the azo-POPs, which is a common challenge in the use of inorganic or organic-inorganic filler materials.

The novel mixed matrix iongel membranes were characterized in terms of gas transport properties, through pure gas permeation experiments (CO_2, N_2, CH_4 and H_2) and the influence of the azo-POP structure in the separation performance was assessed. The morphology, chemical structure and thermal stability of these materials were also investigated through several characterization techniques.

It is worth mentioning that we describe here the synthesis of three new azo-POPs, as well as their characterization in terms of structural properties. Furthermore, to the best of our knowledge, this is the first time that azo-POPs are used as porous fillers in mixed matrix iongel membranes for CO_2 separation.

2. Experimental

2.1. Materials

para-nitrofluorobenzene, *para*-nitrochlorobenzene, sodium hydride (60% in mineral oil), *para*-phenylenediamine, benzidine, 4,4″-diamino-p-terphenyl and dimethylsulfoxide (C_2H_6OS) were purchased from Energy Chemical. Co (China), and used without further purification, unless otherwise noted. The tetra(*p*-nitrophenyl)methane (TNPM) and N,N′,N″, N‴-tetra(*p*-nitrophenyl)phenyldiamine (TNPPDA), N,N′,N″,N‴-tetra(*p*-nitrophenyl)bisphenyldiamine (TNPBPDA), N,N′,N″,N‴-tetra(*p*-nitrophenyl)trisphenyldiamine (TNPTPDA) were synthesized using modified literature methods [46–49]. Poly(ethylene glycol) diacrylate (PEGDA, Mn 575 g mol^{-1}) and 2-hydroxy-2-methylpropiophenone (DAROCUR™, 97 wt% pure) were purchased by Sigma-Aldrich (Portugal). Ionic Liquid 1-ethyl-3-methylimidazolium bis(trifluoromethylsulfonyl) imide ([C_2mim][TFSI], 99 wt% pure) was supplied by Iolitec GmbH (Germany). Carbon dioxide, CO_2 (99.998% purity), nitrogen, N_2 (99.99% purity), methane, CH_4 (99.99% purity) and hydrogen, H_2 (>99.99% purity) gases were supplied by Praxair (Portugal).

2.2. Preparation and characterization of azo-linked porous organic polymers (azo-POPs)

The detailed description of the synthesis of azo-POP monomers can be found in Electronic Supplementary Information (ESI). The synthesis of azo-POPs was carried out using a time-efficient synthetic method reported by Huang et al. [46], via $NaBH_4$-mediated coupling on four-folded monomers containing nitro groups. The synthesis and characterization of azo-POP-1 has already been reported [46]. In the present study, three other monomers (monomer 2, monomer 3 and monomer 4, schematically represented in Fig. 1) containing tetra-nitro groups were prepared by n-arylation of diamines with p-nitrobenzene, in order to synthesize the three new azo-POPs. To obtain the desired azo-POPs, also represented in Fig. 1, a solution of 1 mmol tetranitro monomer in 10 mL of DMF was gradually mixed with a solution of 20 mmol $NaBH_4$ and the resulting mixture was stirred for 1 h at 85 °C. Afterwards, the prepared solution was poured into 100 mL of water and the obtained solid particles were filtered and washed with water and ethanol (3x100 mL). Azo-POP-1, azo-POP-10, azo-POP-11 and azo-POP-12 were obtained as yellow to red solids, with yields over 90%, which structures were confirmed by ^{13}C CP/MS Nuclear Magnetic Resonance (NMR), Fourier Transform Infrared spectroscopy (FTIR) and elemental analysis.

2.3. Adsorption isotherms and morphological characterization of azo-POPs

The morphological characterization of all azo-POPs was performed according to standard procedures. The porous volume and Brunauer-Emmet-Teller (BET) surface area, in the range of $P/P_0 = 0.0–1.0$, were determined by N_2 adsorption/desorption measurements at 77K, using Accelerated Surface Area and Porosimetry System (ASAP 2010). All powdered samples were degassed before each sorption equilibrium experiment, under vacuum at 120 °C for 24h. This ensures that any moisture or contaminants adsorbed on the materials' surface are removed before the experiments.

Carbon dioxide adsorption-desorption experiments were carried out at 273 and 298 K, using a BELSORP-MAX II (BEL Inc., Japan). The azo-POP samples were degassed at 100 °C for 12 h, under vacuum before analysis.

2.4. Preparation of mixed matrix iongel membranes

Bearing in mind our previous results on PEGDA/IL iongels [19], the azo-POP iongel membranes studied in this work were prepared containing 80 wt% IL to maximize their CO_2 loading capacity. Moreover, a low concentration of azo-POP (0.5 wt%) was chosen to make an initial study of the influence of these solid particles on the iongels performances and avoid the need for solvents to disperse the solid particles in the mixture during their preparation.

The mixed matrix iongel membranes were prepared by UV-initiated free radical polymerization. Initially, 80 wt% of IL was mixed with 0.5 wt% (above the total iongel solution) of azo-POP. The obtained solutions were sonicated for 1 h and magnetically stirred overnight to ensure a good dispersion of the solid particles. Afterwards, 20 wt% of PEGDA and around 3 wt% (relative to PEGDA) of DAROCUR™ as photo initiator were added, and the solutions were left stirring until they were completely homogeneous. The resulting mixtures were casted between two Rain-X™ coated quartz plates, with a 120 μm spacer in between and exposed to a UV light using a UVC-5 UV Curing Conveyor System with 800 mW cm^{-2}, at a wavelength of 365 nm. The distance from sample to lamp was 1 cm and the belt speed was set at 1 m min^{-1}. The resulting iongels were peeled off from the plates and characterized. Fig. 2 shows a schematic illustration of the preparation of mixed matrix iongels containing azo-POP.

Composite membranes were prepared to carry out the gas permeation experiments without compromising the mechanical integrity of the iongels. The iongel was supported on a pre-wetted porous polyamide (PA) filter (Sartorius™, supplied by Fisher Scientific) with a pore size of 0.22 μm. The support was immersed in deionized water before the solution was casted on top of it, in order to minimize the pore filling from the iongel solution to the porous support. The chosen hydrophilic PA support was found to be compatible with the iongel solution, assuring a good adhesion between the two layers.

2.5. Scanning Electron Microscopy (SEM)

Scanning Electron Microscopy images of the surface and cross section of the prepared self-standing iongels and composite membranes (iongel supported onto porous polyamide filter) were acquired using an analytical JEOL 7001F scanning electron microscope (FEG-SEM),

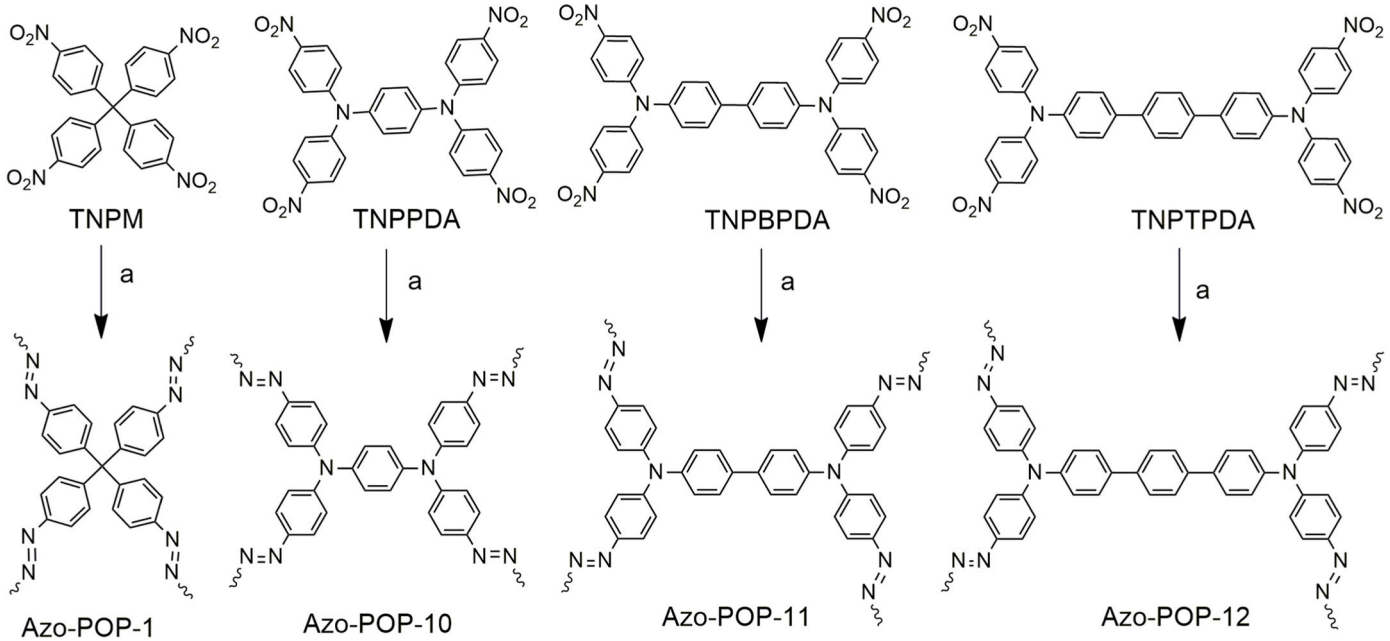

Fig. 1. Synthesis of the different azo-POPs from the corresponding monomers. Condition a corresponds to: NaBH4, DMF, 0.5h at 85 °C.

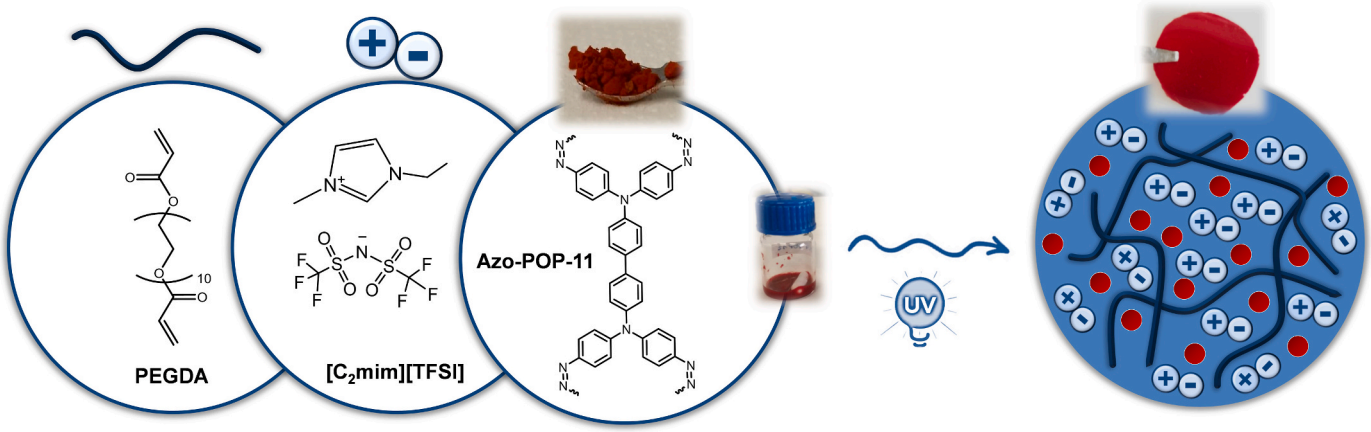

Fig. 2. Schematic illustration of the preparation of mixed matrix iongel membranes containing azo-POP.

equipped with a field emission gun operated at 15 kV. All samples were coated with a thin Pd/Au layer to induce charge under the electron beam.

2.6. Fourier Transform Infrared spectroscopy analysis (FTIR)

FTIR analysis was performed for all the iongel membranes and azo-POPs to confirm their chemical structure, as well as to determine if there are any interactions being established between the materials used. The FTIR spectra were acquired in a PerkinElmer Spectrum two spectrometer. The spectra were collected using 10 scans, from 4000 to 400 cm^{-1}, with a resolution of 4 cm^{-1}.

2.7. Contact angle measurements

The contact angle of all the prepared iongel membranes was measured to evaluate their hydrophilic/hydrophobic nature. A drop of distilled water was manually deposited on the surface of each membrane sample, and three replicates were performed to obtain the mean contact angle. For each replicate, 10 frames were acquired, with an interval of 1 s between each, and all images were processed by CAM100 (KSV) software, where the water drop was fitted to mathematical functions.

2.8. Thermogravimetric analysis (TGA)

Thermogravimetric analysis was carried out using a TA Instrument model TGA Q50. Iongel membranes and azo-POPs samples of around 10 mg were heated from room temperature to 600 °C, at a constant heating rate of 10 °C min^{-1}, under a nitrogen flow of 40 mL min^{-1}, to prevent thermo oxidative degradation of the samples. The obtained data was analysed using a Universal Analysis 4.5A software to determine the onset temperature, (T_{onset}), defined as the temperature at which the baseline slope changes and degradation temperature, (T_{dec}), defined as the temperature at 50% weight loss.

2.9. Mechanical properties

The mechanical properties of the prepared composite membranes (iongel supported onto porous polyamide filter) were evaluated through tensile tests, using a TMS-Pro texture analyser, where the samples were stretched until their rupture. All samples were prepared with 1.5 × 6 cm and thickness of around 200 μm. Each sample was placed between two testing clamps and the testing speed was set at 1 mm s^{-1}, until the rupture of the sample. For each sample, at least four replicates were performed and the mean values of the tension at break, deformation at break and Young's modulus were determined.

2.10. Single gas permeation experiments

Gas permeation experiments were carried out for pure CO_2, N_2, CH_4 and H_2, at 0.7 bar and 30 °C, using an experimental setup, fully described elsewhere [8]. The system is composed by a stainless-steel cell with two similar compartments, designated as feed and permeate, separated by the membrane. The detailed procedure to carry out a gas permeation experiment can be found in our previous work [8]. The permeability of a pure gas through the membrane was calculated from the obtained pressure data over time, on both compartments, according to the following equations [50].

$$\frac{1}{\beta}\ln\left(\frac{\left[p_{feed}-p_{perm}\right]_0}{\left[p_{feed}-p_{perm}\right]}\right)=\frac{1}{\beta}\ln\left(\frac{\Delta p_0}{\Delta p}\right)=P\frac{t}{l} \quad (1)$$

where p_{feed} and p_{perm} are the pressures (bar) in the feed and permeate compartments, respectively, P is the membrane permeability (m^2s^{-1}, where 1 Barrer = $1x10^{-10}$ cm^3 cm $cm^{-2}.s^{-1}.cmHg^{-1} = 8.3x10^{-13}$ m^2 s^{-1} [50]), t is the time (s) and l is the membrane thickness (m). β (m^{-1}) is a geometric parameter, characteristic of the geometry of the cell, given by:

$$\beta = A\left(\frac{1}{V_{feed}}+\frac{1}{V_{perm}}\right) \quad (2)$$

where A is the membrane area (m^2) and V_{feed} and V_{perm} are the volumes (m^3) of the feed and permeate compartments, respectively. The gas permeability is obtained from the slope represented by ploting $\frac{1}{\beta}\ln\left(\frac{p_0}{p}\right)$ versus $\frac{t}{l}$.

The ideal gas selectivity was calculated by dividing the permeabilities of the two different gases (A and B), according to the following equation:

$$\alpha_{A/B}=\frac{P_A}{P_B} \quad (3)$$

It should be noted that, in this work, the permeability data obtained from Eq. (1), as well as the thickness considered for these calculations, are related to the global permeability of the membrane, considering the polymeric support and the iongel layer.

To understand the contribution of the iongel layer alone to the gas transport of the membrane, the iongel permeability was calculated using the resistance in series model (RSM) [51,52]. According to the RSM, the gas transport on a layered membrane and the electric current flow in the serial connection to conductors are equivalent since the different layers of a composite membrane can be described in terms of their resistance to gas transport. The resistance (R) to the gas flow is proportional to the thickness (l) and inversely proportional to the permeability (P) and surface area (S), and the total resistance is equal to the sum of resistances

originating from each layer.

The resistance of a specific layer can be calculated using the following equations:

$$R = \frac{l}{P.S} \tag{4}$$

$$R_t = R_i + R_s \tag{5}$$

$$\frac{l_t}{P_t.S} = \frac{l_i}{P_i.S} + \frac{l_s}{P_s.S} \tag{6}$$

The permeability of the double layer composite membrane is described by the following equation:

$$P_t = \frac{(l_i + l_s).P_i.P_s}{(P_s.l_i) + (P_i.l_s)} \tag{7}$$

Consequently, by knowing the gas permeability of the composite membrane and pre-wetted support layer (s) obtained from Equation (1), as well as the respective thickness of each of these layers, it is possible to predict the permeability of the iongel layer (i). In this work, even though porous supports were used in the preparation of the membranes, it was observed that, due to the pre-wetting step, they offered resistance to the gas transport, which did not occur when the supports were dry. For that reason, gas permeation measurements for all gases were also performed on the pre-wetted support to determine the permeability, Ps, of this layer.

For the gases studied in this work, the permeability of the double layer structure can be described by the following equations:

$$P_t^{CO_2} = \frac{(l_i + l_s).P_i^{CO_2}.P_s^{CO_2}}{(P_s^{CO_2}.l_i) + (P_i^{CO_2}.l_s)} \tag{8}$$

$$P_t^{N_2} = \frac{(l_i + l_s).P_i^{N_2}.P_s^{N_2}}{(P_s^{N_2}.l_i) + (P_i^{N_2}.l_s)} \tag{9}$$

$$P_t^{CH_4} = \frac{(l_i + l_s).P_i^{CH_4}.P_s^{CH_4}}{(P_s^{CH_4}.l_i) + (P_i^{CH_4}.l_s)} \tag{10}$$

$$P_t^{H_2} = \frac{(l_i + l_s).P_i^{H_2}.P_s^{H_2}}{(P_s^{H_2}.l_i) + (P_i^{H_2}.l_s)} \tag{11}$$

where $P_i^{CO_2}$, $P_i^{N_2}$, $P_i^{CH_4}$ and $P_i^{H_2}$ are the CO_2, N_2, CH_4 and H_2 permeability of the iongel layer, and $P_s^{CO_2}$, $P_s^{N_2}$, $P_s^{CH_4}$ and $P_s^{H_2}$ are the CO_2, N_2, CH_4 and H_2 permeability of the support layer, respectively.

The ideal selectivity of each gas pair can be calculated, for the composite membrane or for each layer, by dividing the correspondent permeability of the more permeable species (CO_2) by the permeability of the least permeable species (N_2, CH_4, and H_2), according to the previously described equation (3).

3. Results and discussion

3.1. Azo-POPs characterization and N_2 adsorption isotherms

In this work, four different azo-POPs were synthesized according to Fig. 1, azo-POP-1 and the new porous polymers azo-POP-10, azo-POP-11 and azo-POP-12. The structures of azo-POPs were evidenced by their solid-state ^{13}C CP/MS NMR (see Fig. S3, ESI), which showed the common chemical shifts in the range of 100–160 ppm for sp^2 carbons and characteristic broad peak of –C–N═N– bond at 152 ppm. In the case of azo-POP-1, the peak around 65 ppm indicates the presence of a quaternary carbon. The exact ratio between the masses of C and N for azo-POPs was determined by elemental analysis (see Table S1, ESI), and the obtained data showed that C/N ratio of all the azo-POPs samples is well consistent with theoretical values [43,53].

Looking at the N_2 sorption isotherms of the prepared azo-POP-10, azo-POP-11 and azo-POP-12 shown in Fig. 3, the rapid uptake at low pressure (0–0.1 bar) indicates the presence of permanent micropores. The apparent hysteresis between adsorption and desorption suggests that the prepared azo-POPs are networks enclosing both meso and micropores, which are assigned to the pore network effects [54,55]. The same behaviour had already been observed for azo-POP-1 in a previous work [46]. The BET surface area and porous volume obtained for the prepared azo-POPs are displayed in Table 1. The BET surface areas were calculated as 1100 $m^2\ g^{-1}$ (azo-POP-1), 439 $m^2\ g^{-1}$ (azo-POP-10), 478 m^2g^{-1} (azo-POP-11) and 298 $m^2\ g^{-1}$ (azo-POP-12), while the porous volumes were obtained between 0.57 cm^3g^{-1} for azo-POP-1 to 0.29 cm^3g^{-1} for azo-POP-12. These BET SA are generally higher than those reported for azo-POP-7, azo-POP-13 and azo-POP-14 and within the range of values obtained for azo-POP-2 and azo-POP-3 [56,57]. Moreover, it was found that azo-POP-1 presented the most narrow pores (2.8 nm, average), while azo-POP-12 encloses the biggest pores in its structure (around 7.8 nm), compared to the other azo-POPs studied.

3.2. Single gas CO_2 adsorption isotherms

Fig. 4 illustrates the single gas CO_2 adsorption isotherms obtained at 273 and 298 K, for synthesized azo-POP-1, azo-POP-10, azo-POP-11 and azo-POP-12. All sorption isotherms are type I, according to the IUPAC classification, which is characteristic of microporous materials [58]. Except for azo-POP-1 at 298 K, where a small hysteresis can be observed, no hysteresis were found for the remaining isotherm curves, showing a completely reversible behavior and possible full regeneration of the materials after the sorption experiments. The smooth adsorption-desorption cycles show that the interactions between the azo-POPs and CO_2 molecules are weak enough to regenerate the materials. This finding is of great importance for cyclic adsorption gas separations processes, where the adsorbent material should be able to fully regenerate to prevent residual adsorbed gas onto the material.

The adsorption capacities obtained at 273 K, were 2.3 mmol g^{-1} for azo-POP-1, 1.51 mmol g^{-1} for azo-POP-10, 0.66 mmol g^{-1} for azo-POP-11 and 1.55 mmol g^{-1} for azo-POP-12, which decrease at 298 K to 1.95 mmol g^{-1}, 0.82 mmol g^{-1}, 0.37 mmol g^{-1} and 0.91 mmol g^{-1}, respectively. As expected, the adsorption capacity decreases with increasing temperature since this is an exothermic process. The adsorption capacity obtained for the synthesized azo-POPs are lower than the values obtained for other azo-POPs previously reported in the literature, having similar structures [53,59]. However, their performance as fillers in membranes for gas separation was not assessed.

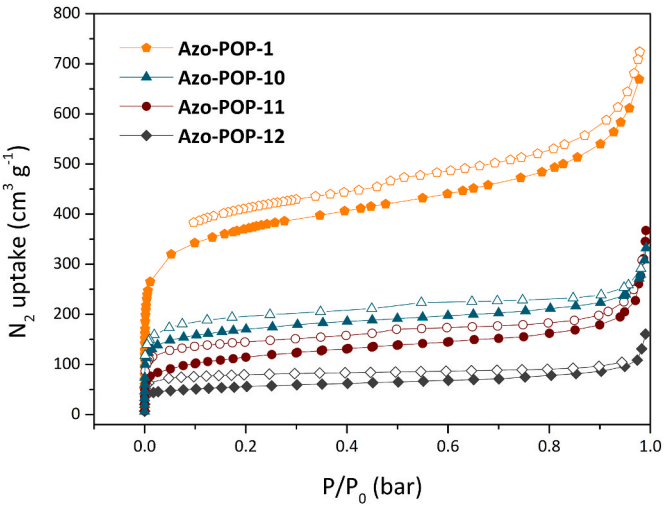

Fig. 3. N_2 sorption isotherms of the prepared azo-POPs.

Table 1
Morphological characterization of the azo-POPs studied in this work.

Azo-POP	BET surface area (m^2 g^{-1})	Porous volume (cm^3 g^{-1})	Mean Pore size (nm)
Azo-POP-1	1100	0.57	2.8
Azo-POP-10	439	0.35	3.4
Azo-POP-11	478	0.34	3.6
Azo-POP-12	298	0.29	7.8

3.3. Membrane preparation and characterization

As illustrated in Fig. 2 and described in the experimental section, the mixed matrix iongel membranes were prepared by UV-photopolymerization of PEGDA in the presence of 80 wt% of IL and 0.5 wt% of azo-POP. We selected this PEGDA/IL formulation based on our previous work. The powdery azo-POPs were easily dispersed in the liquid PEGDA/IL mixture before photopolymerization without the need of additional organic solvent.

3.3.1. Scanning Electron Microscopy

As a typical example, Fig. 5a and b shows the SEM images of the surface and fractured cross-section of the self-standing iongel membrane containing the azo-POP-11. A non-porous and defect free membrane morphology was obtained, since no deformations, agglomerations or phase separation were detected. Such morphology indicates not only a good miscibility between the different components, but also a good dispersion of the azo-POP particles in the iongel membrane. It should be noted that the reliefs seen in the cross-section image are probably due to the plastic deformation caused by liquid nitrogen during the fracturing process. The same type of morphology was found for all the iongel membranes prepared in this work. Fig. 5c and d shows the SEM images of the respective composite membrane, composed by the PEGDA-80 TFSI-0.5 POP-11 iongel and the porous polyamide support. Similarly, the iongel layer of the composite membrane also presents a dense and defect-free surface, while in the cross-section image it is possible to distinguish the support (top) from the iongel layer (bottom).

3.3.2. Fourier Transform Infrared spectroscopy

The chemical structure of the azo-POPs and prepared iongel membranes were confirmed by FTIR spectroscopy, as shown in Fig. S4 (ESI) and Fig. 6, respectively.

The presence of the azo group in azo-POP-1, azo-POP-10, azo-POP-11 and azo-POP-12 (Fig. S4, ESI) was confirmed by the absorption peaks at 1480 and 1410 cm^{-1}, corresponding to the N═N stretching vibrations. The peaks observed at 1270 and 1305 cm^{-1} are attributed to the C–N stretching vibrations of the aromatic compounds present in the azo-POP structures [46].

In Fig. 6, the presence of PEGDA in the iongel can be confirmed by the peaks at 1730 cm^{-1}, arising from the C═O symmetric stretching and the bands at around 2878 and 2940 cm^{-1}, attributed to the C–H stretching. Moreover, the absence of visible peaks at 1619 cm^{-1} and 1635 cm^{-1} (C═C asymmetric and symmetric stretching, respectively), attributed to the presence of terminal acrylate groups from PEGDA, confirms the occurrence of the polymerization reaction [19]. The peak at 1460 cm^{-1} and the bands at 3120 and 3160 cm^{-1} are assigned to the CH_3 bending vibrations and CH_2 stretching vibrations, respectively, originated from the imidazolium-based cation of the IL. On the other hand, the bands at 1049 cm^{-1}, 1132 cm^{-1}, 1178 cm^{-1} and 1343 cm^{-1} are typical of the TFSI anion [19]. The characteristic peaks of azo-POPs, described above, were not detected in the iongels spectra, due to the low azo-POP content in the iongel or possible overlapping of peaks.

3.3.3. Contact angle measurements

The water contact angle of each iongel membrane sample was measured, and the respective mean values and corresponding errors are displayed in Fig. 7. The PEGDA-80 TFSI iongel presents the highest water contact angle at 61.9°, and this value decreases upon the incorporation of different azo-POPs, down to 42.5° for PEGDA-80 TFSI-0.5 POP-1, suggesting that the addition of azo-POPs accentuates the hydrophilic character of these materials. For the different iongels containing azo-POPs, the water contact angles are similar, probably because the azo-POP structures are also similar between them and thus, the POPs used do not have a major impact in this parameter.

3.3.4. Thermogravimetric analysis

Fig. 8 presents the TGA profiles of the prepared iongel membranes. The mixed matrix iongels containing the different azo-POPs present a similar behaviour when compared to that of the PEGDA-80 TFSI iongel. Until around 200 °C, only trapped moisture is removed. Considering that PEGDA has a lower thermal stability compared to the neat [C_2mim][TFSI] IL, the PEGDA-TFSI iongel exhibits T_{onset} and T_{dec} values between those of the neat materials. After the incorporation of the different azo-

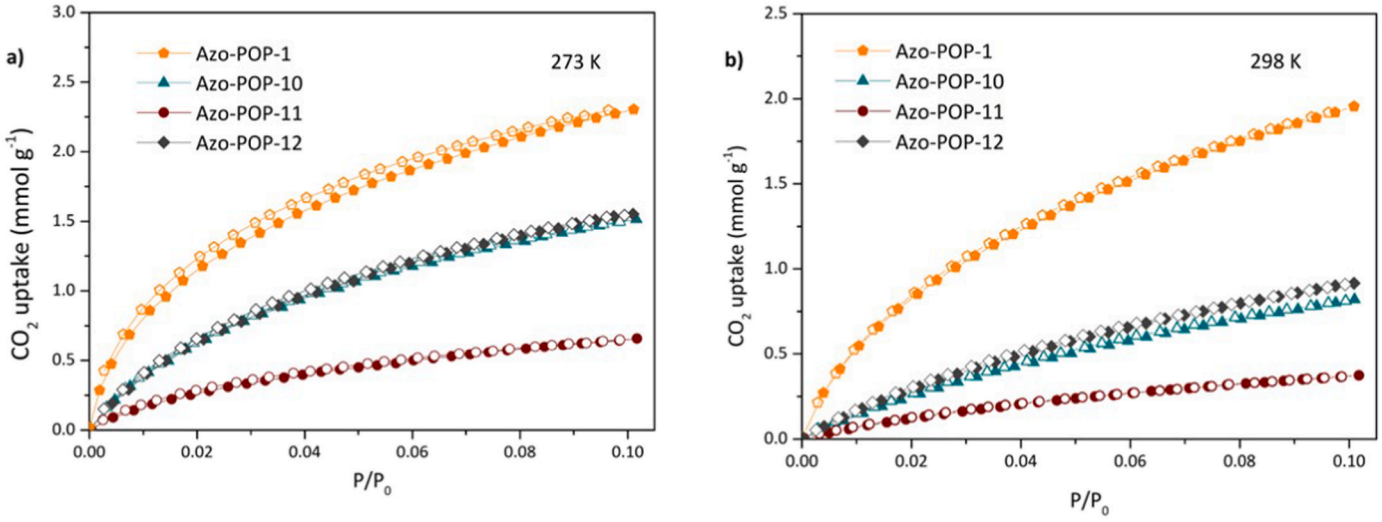

Fig. 4. CO_2 adsorption isotherms in azo-POP-1, azo-POP-10, azo-POP-11 and azo-POP-12, at 273 and 298 K. Closed and open symbols denote adsorption and desorption data, respectively.

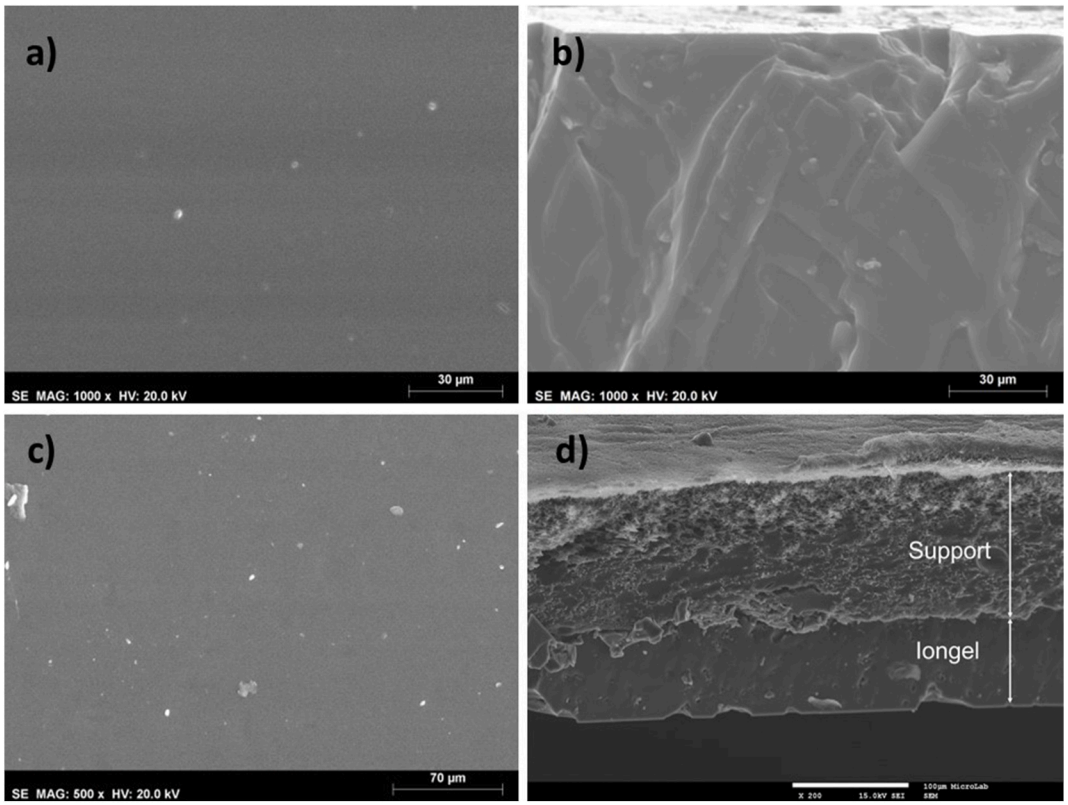

Fig. 5. SEM images of the surface (a,c) and cross section (b,d) of the self-standing (a,b) and composite (c,d) iongel membranes composed by PEGDA-80 TFSI-0.5 POP-11.

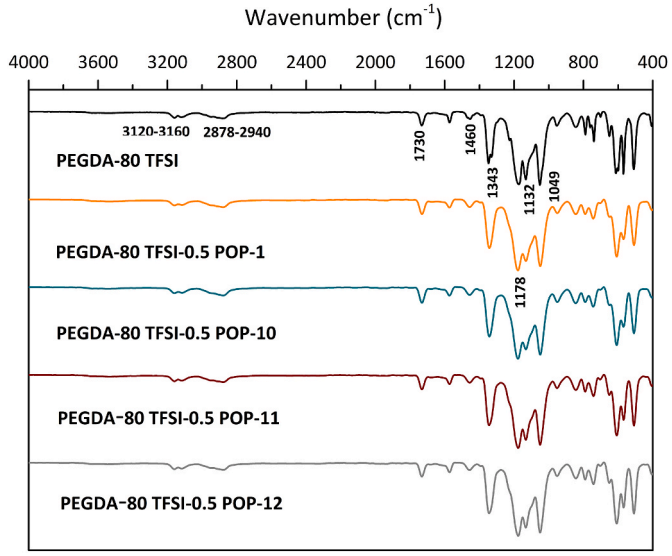

Fig. 6. FTIR spectra of the PEGDA-80 TFSI iongel and the different mixed matrix iongel membranes containing different azo-POPs.

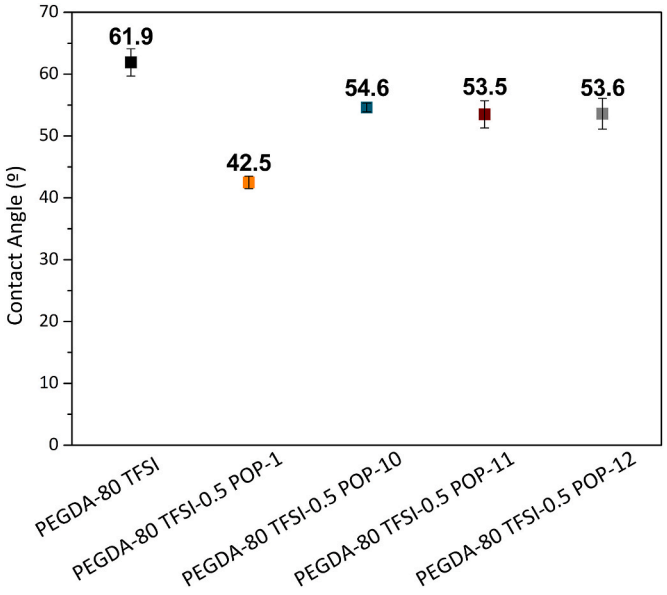

Fig. 7. Water contact angles obtained for the PEGDA-80 TFSI iongel and the mixed matrix iongel membranes containing different azo-POPs.

POPs, both T_{onset} and T_{dec}, presented in Table S2 (ESI), decreased from 388 °C for the PEGDA-80 TFSI to 337 °C for the PEGDA-80 TFSI-0.5 POP-1 iongel. Above these temperatures there is a continuous weight loss, which results in the total degradation of the iongels. The decrease observed after the incorporation of azo-POPs is attributed to a lower thermal stability of these materials, compared to PEGDA or the IL. The T_{onset} of azo-POP-1, azo-POP-10, azo-POP-11 and azo-POP-12 were detected at 241, 285, 310 and 290 °C, respectively, as observed in Fig. S5 (ESI) [46]. Nonetheless, the TGA results here presented confirm that the proposed mixed matrix iongel membranes containing azo-POPs possess a suitable thermal stability within the typical temperature range of the CO_2/N_2, CO_2/CH_4 and CO_2/H_2 streams, with weight losses <3 wt % up to 200 °C.

3.3.5. Mechanical properties

Table 2 shows the tension at break, deformation at break and

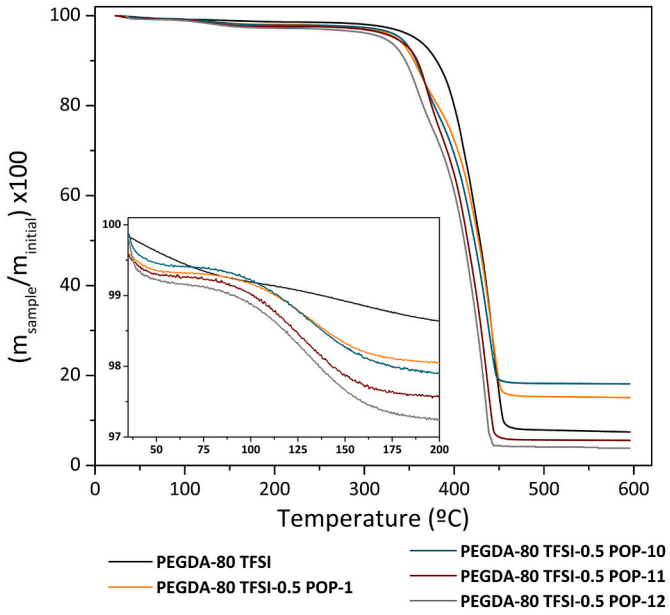

Fig. 8. Thermogravimetric profiles of the PEGDA-80 TFSI iongel and the mixed matrix iongel membranes containing different azo-POPs.

Young's modulus obtained for all composite iongel membranes, in which the iongel is supported on top of a porous polyamide filter. The self-standing mixed matrix iongel membranes were too mechanically fragile to be tested since, they broke easily when placed between the testing clamps of the equipment. Thus, only the porous polyamide support and the respective composite iongel membranes, were tested. The results concerning the tension at break and Young's Modulus show that the polymeric support alone can withstand a higher stress before breaking and has a higher resistance to elastic deformation, compared to the composite iongel membranes. The pre-wetting step and the casting of the iongel solution on the polyamide support surface may decrease the stiffness of this layer, by acting as a plasticizer that reduces the entanglement and bonding between molecular chains, resulting in the variations of the mechanical parameters observed in Table 2 [60,61]. It was also observed that, as the tension increased, the iongel layer began to crack while the support was stretched, finally resulting in its rupture. This happens because the iongel layer is mechanically weaker when compared to the polyamide support. Small cracks in the iongel started to be observed during the plastic deformation region of the samples. Looking at the data obtained for the composite iongel membranes, it is possible to perceive that the composition of the azo-POP iongel layer has no significant impact in the mechanical parameters determined from these experiments, since the main contribution to the membrane's strength is made by the support layer. This explains the use of a support layer to provide mechanical resistance for the mixed matrix iongel membranes containing azo-POPs during the gas permeation tests. Even though the iongel layers started to crack at a lower tension, they did not detach from the polyamide support, showing a good adhesion between the two materials and also the successful preparation of these composite membranes.

3.3.6. *Pure gas permeation experiments*

Pure gas permeation experiments were carried out for CO_2, N_2, CH_4 and H_2, to study the influence of the incorporation of different azo-POPs on the permeability and selectivity of mixed matrix iongel membranes. It is important to emphasize once again that, to the best of our knowledge, this is the first time that a class of POPs is incorporated in iongel membranes for gas separation.

The gas transport in mixed matrix iongel membranes follows the same mechanism of other dense membranes, where the permeability is a combined effect of the gas diffusivity and solubility (P═S × D) and the incorporation of porous materials has a direct influence on these parameters. For nonpolar gases, such as CH_4, N_2 and H_2, the solubility depends primarily on the properties of the gas molecules, while for CO_2 this coefficient is more dependent on the membrane material and its interactions with the gas molecules. Moreover, the presence of specific functional groups can help increase the solubility coefficient. On the other hand, the diffusivity is primarily governed by the gas molecule size and the free volume in the membrane structure. The porosity induced by the incorporation of porous materials, such as azo-POPs, can restrict or facilitate the diffusion of gas molecules, depending on their size.

Table S3 (ESI) presents the global CO_2 permeabilities and the CO_2/N_2, CO_2/CH_4 and CO_2/H_2 ideal selectivities of the prepared composite membranes, considering the iongel deposited on top of the polyamide support. To better understand the separation performance of the mixed matrix iongel layer, Table 3 presents the CO_2 permeabilities and the CO_2/N_2, CO_2/CH_4 and CO_2/H_2 ideal selectivities of the iongel layers, calculated according to Equation (8) and Equation (3), respectively, and the following discussion will be focused on these results.

From Table 3, it can be seen that the CO_2 permeability is favoured by the incorporation of azo-POP in the iongel, even at such a low concentration (0.5 wt%), since these membranes were able to outperform the one composed by only PEGDA and 80 wt% of IL. This improvement in CO_2 permeability results from the incorporation of an extra porous network provided by the azo-POPs, the physical nature of their pores and the azo functional groups present in their structures, as previously revealed by both theoretical and experimental studies [45,53,59]. It has been demonstrated that porous frameworks with nitrogen-rich functionalities provide "CO_2-philic" properties to the membrane and high CO_2 uptake capacity. These features are believed to arise from enhanced CO_2-framework interactions through strong dipole-quadrupole interactions. Azo groups can act as a Lewis basic site, while the carbon atom in CO_2 acts as an acid, originating dipole/quadrupole interactions between the two sites, thus resulting in a higher affinity of the azo-POP

Table 2
Tension at break, deformation at break and Young's modulus of the polymeric PA support and the different mixed matrix iongel membranes prepared in this work.

Sample	Tension at break (MPa)	Deformation at break (%)	Young's Modulus (MPa)
Porous PA support	21.1 ± 0.3	19.6 ± 0.4	5.8 ± 0.1
PEGDA-80 TFSI	12.1 ± 0.9	16.5 ± 0.9	3.1 ± 0.2
PEGDA-80 TFSI-0.5 POP-1	13.3 ± 1.3	16.7 ± 1.7	3.3 ± 0.3
PEGDA-80 TFSI-0.5 POP-10	12.2 ± 0.6	24.6 ± 0.9	2.5 ± 0.1
PEGDA-80 TFSI-0.5 POP-11	13.5 ± 1.6	16.7 ± 0.3	3.4 ± 0.2
PEGDA-80 TFSI-0.5 POP-12	13.1 ± 1.5	19.6 ± 2.0	2.9 ± 0.3

Table 3
CO_2 permeability and CO_2/N_2, CO_2/CH_4 and CO_2/H_2 ideal selectivities of the mixed matrix iongel layers containing different azo-POPs.

Iongel layer	P_i CO_2 (barrer)	α_i (CO_2/N_2)	α_i (CO_2/CH_4)	α_i (CO_2/H_2)
PEGDA-80 TFSI	62.3 ± 1.6	16.8 ± 0.5	10.2 ± 0.2	6.20 ± 0.5
PEGDA-80 TFSI-0.5 POP-1	90.6 ± 2.7	27.8 ± 0.4	10.5 ± 0.2	12.1 ± 0.8
PEGDA-80 TFSI-0.5 POP-10	79.0 ± 2.0	19.0 ± 1.0	11.5 ± 0.3	11.4 ± 0.6
PEGDA-80 TFSI-0.5 POP-11	79.8 ± 2.8	40.5 ± 2.1	12.0 ± 0.2	11.0 ± 0.2
PEGDA-80 TFSI-0.5 POP-12	68.0 ± 1.5	53.1 ± 2.9	9.9 ± 0.2	12.1 ± 0.5

pore surface for CO_2 [44]. It is also interesting to see that, for the mixed matrix iongel membranes, the CO_2 permeability is higher when the contact angle is lower (Fig. 7), as the solubility of CO_2 in more hydrophilic materials is generally higher than in less hydrophilic/hydrophobic ones.

The highest CO_2 permeability was achieved for the iongel membrane with azo-POP-1 (90.6 barrer), while the lowest was obtained for the one with azo-POP-12 (68.0 barrer). These CO_2 permeability values follow a trend similar to that of the BET surface area (1100 $m^2\ g^{-1}$, and 298 $m^2\ g^{-1}$, respectively) and porous volume (0.57 $cm^3\ g^{-1}$ and 0.29 $cm^3\ g^{-1}$, respectively) parameters obtained for these materials (Table 1). Moreover, stronger CO_2-framework interactions are expected in azo-POPs having more narrow pores, due to a higher number of interactions between the adsorbed CO_2 molecules and the pore walls [41]. Additionally, from the CO_2 adsorption experiments, it is also possible to conclude that the higher CO_2 permeability of the iongel containing azo-POP-1 is favoured by the higher adsorption capacity of this material. Therefore, the narrower pores of azo-POP-1 combined with its higher surface area and CO_2 uptake capacity leads to the highest CO_2 permeability. Looking at the CO_2 uptakes obtained for the studied azo-POPs, it is possible to conclude that the CO_2 permeabilities of the respective iongels do not follow the same trend. This indicates that the gas transport across the iongel is primarily governed by the porosity parameters of the organic fillers, rather than their intrinsic CO_2 adsorption capacity.

Regarding the ideal selectivities obtained for the prepared mixed matrix iongel membranes, the CO_2/CH_4 and CO_2/H_2 separations show similar results, which are considerably lower than the ones obtained for the CO_2/N_2 separation. It is known that CH_4 is a more soluble gas, compared to N_2 and that H_2 has the smallest gas molecules (2.9 Å), among all studied gases. A higher solubility of CH_4 and diffusivity of H_2 gas molecules, compared to N_2, promotes their permeability, which may lead to a lower selectivity. Nonetheless, for all gas pairs considered, the selectivities of the azo-POP-containing iongels are higher than those obtained for the neat PEGDA-80 TFSI iongel. The iongel containing azo-POP-12 shows the highest CO_2/N_2 selectivity, originating from its low BET surface area, which leads to a low N_2 uptake. Even though azo-POP particles induce a higher porosity in the iongels structure, facilitating the diffusion of the gas molecules, their high affinity towards CO_2 overcomes this effect, increasing the separation efficiency. The higher CO_2/N_2 selectivities in the mixed matrix iongel membranes are a direct consequence of the presence of the azo groups in the POPs structures. The differences in the affinity of azo functional groups towards N_2 and CO_2 are the key factor for the improved selectivity. Patel and co-workers showed, though Monte Carlo simulations, that the binding affinity of the azo groups towards N_2 (9.0 kJ mol^{-1}) is considerably lower than for CO_2 (17.0 kJ mol^{-1}) [53]. These findings unveil the possibility of designing highly-selective azo-POPs to be used as fillers in membranes for gas separations.

In order to better understand the overall separation performance of the prepared mixed matrix iongel membranes containing azo-POPs, the experimental data obtained from this work were plotted against the well-known upper bound limits for CO_2/N_2 (Fig. 9 a), CO_2/CH_4 (Fig. 9 b) and CO_2/H_2 (Fig. 9 c) separations, at 30 °C, where the ideal selectivity for each separation is represented as a function of the CO_2 permeability [62]. It is worth mentioning that the first upper bound limits developed based on experimental data for the H_2/CO_2 separation, at low temperatures, considered that the permeability of H_2 was much higher than that of CO_2 [63]. However, it is known that depending on the materials and their interactions with the gas molecules, it is also possible to achieve a higher permeability for CO_2 compared to H_2, as we show in this work, which led to the development of a new upper bound limit for CO_2/H_2 [62]. The available data reported for other three-component membranes, containing high IL content (> 60 wt%) and other third component solid materials, such as silica nanoparticles [16,64,65], zeolites [23], and MOFs [20], at higher concentrations (between 8 and 15 wt%), is also plotted against the upper bound limits, in order to provide a general idea of the performance of the novel mixed matrix iongel membranes containing azo-POPs proposed herein.

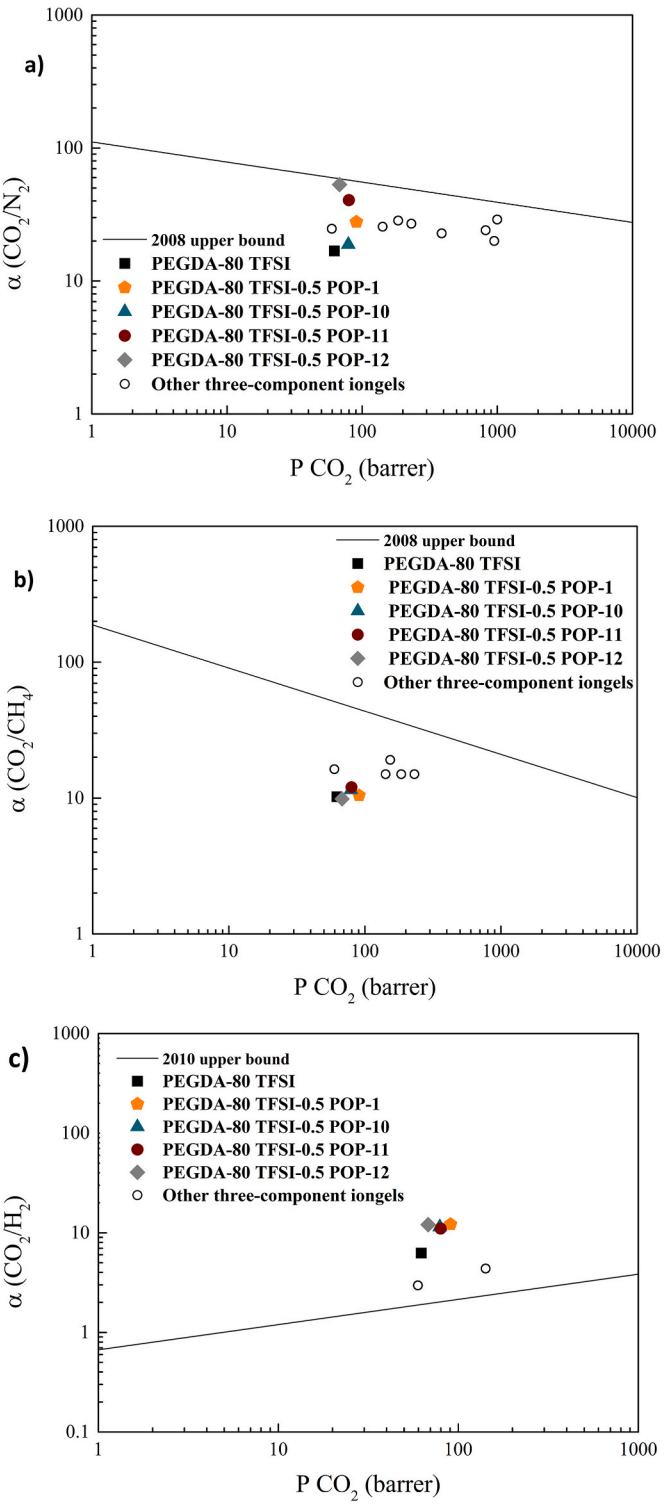

Fig. 9. (a) CO_2/N_2, (b) CO_2/CH_4, (c) CO_2/H_2 ideal selectivities of the prepared mixed matrix iongel membranes containing different azo-POPs as a function of CO_2 permeabilities. Literature data are also illustrated for comparison purposes.

Looking at Fig. 9 a), the experimental results of this work come closer to the CO_2/N_2 upper bound limit, after the incorporation of the different azo-POPs, with the mixed matrix iongel membranes based on azo-POP-11 and azo-POP-12 showing the best results. It is also possible to conclude that overall, the CO_2 permeabilities obtained with third

component solid materials, such as silica nanoparticles [16,64,65], zeolites [23] and MOFs [20] are higher, compared to those obtained in this work with azo-POPs. However, the CO_2/N_2 ideal selectivities are generally higher, bringing the experimental results closer to the CO_2/N_2 upper bound limit than those reported in the literature. In contrast, for the CO_2/CH_4 separation, depicted in Fig. 9 b), the relation between permeability and selectivity found in the mixed matrix iongel membranes containing azo-POPs is not as promising as it is for the other membranes with higher filler concentrations, mainly due to lower ideal selectivity. Interestingly, the exact opposite behaviour was observed for CO_2/H_2 separation (Fig. 9 c), where even the unfilled iongel composed of only PEGDA and IL exhibited a remarkable performance, and all experimental points were able to overcome the respective upper bound limit.

It is also worth noting that the azo-POP concentration used in the mixed matrix iongel membranes (0.5 wt%) is considerably low when compared to the literature data available for iongels containing silica [16,64,65], zeolites [23] and MOFs [20] (between 8 and 15 wt%). Therefore, we can expect that an increase in the azo-POP loading will probably improve the iongels' permeabilities [11,66,67].

4. Conclusions

Mixed matrix iongel membranes, which are entirely composed of organic materials (PEGDA, 80 wt% $[C_2mim][TFSI]$ IL and four different azo-POPs) were successfully prepared, for the first time, by a fast and simple solvent-free UV polymerization process. The SEM analysis demonstrated that dense and defect-free mixed matrix iongel membranes with a good dispersion of azo-POP particles were obtained. All the iongel membranes presented high thermal stabilities (>330 °C). Furthermore, the pure gas permeation experiments showed that with only 0.5 wt% of azo-POP, it was possibly to improve both CO_2 permeability (from 62.3 to 90.6 barrer) and CO_2/N_2, CO_2/CH_4 and CO_2/H_2 ideal selectivities, mainly due to the "CO_2-philic" nature of azo-POPs. In fact, it was found that the azo-POP structure had a significant influence on the CO_2/N_2 ideal selectivity, since the "N_2-phobicity" of these materials is strictly dependent on porosity parameters. Remarkably, all the prepared iongels were able to surpass the CO_2/H_2 upper bound limit.

Overall, the results of this work clearly indicate that the incorporation of different azo-POPs in iongels with high IL content is a promising strategy that should be taken into consideration regarding the design of membrane materials with improved CO_2 separation properties. Moreover, besides the separation performance, it is also worth highlighting the straightforward and solvent-free method used in the preparation of these mixed matrix iongel membranes, as well as the novelty in the combination of the different organic materials.

Future work will be focused on evaluating the gas separation performance of these mixed matrix iongel membranes at experimental conditions that mimic those of industrial gas streams, in terms of composition, temperature, pressure and water vapour content.

Author Statement

Conceptualization: L.C. Tomé, L.A. Neves, M-H. Huang; Investigation: A.R. Nabais, S. Ahmed, M. Younis, J.X. Zhou, J.R. Pereira; Visualization: A. R. Nabais; Writing – original draft: A. R. Nabais; Writing – review and editing: L. A. Neves, L. C. Tomé, M-H. Huang, F. Freitas, D. Mecerreyes, J.G. Crespo; Supervision: L.A. Neves, L.C. Tomé, D. Mecerreyes, J.G. Crespo, M-H. Huang; Resources: L.A. Neves, L.C. Tomé, D. Mecerreyes, J.G. Crespo, F. Freitas.

Declaration of competing interest

The authors declare that they have no known competing financial interests or personal relationships that could have appeared to influence the work reported in this paper.

Data availability

Data will be made available on request.

Acknowledgements

Ana R. Nabais and Liliana C. Tomé acknowledge Fundação para a Ciência e a Tecnologia (FCT/MCTES) for financial support through PhD grant (SFRH/BD/136963/2018), and assistant researcher contract under Scientific Employment Stimulus (2020.01555.CEECIND), respectively. This work was supported by Associate Laboratory for Green Chemistry – LAQV (UIDB/50006/2020 and UIDP/50006/2020), the Research Unit on Applied Molecular Biosciences - UCIBIO (UIDP/04378/2020 and UIDB/04378/2020) and the Associate Laboratory Institute for Health and Bioeconomy - i4HB (LA/P/0140/2020), which are financed by national funds from FCT/MCTES. The authors also thank the National Natural Science Foundation of China (No. 21772013) and Beijing Natural Science Foundation (No. 2202049) for generous support.

Appendix A. Supplementary data

Supplementary data to this article can be found online at https://doi.org/10.1016/j.memsci.2022.120841.

References

[1] J. Xu, Z. Wang, Z. Qiao, H. Wu, S. Dong, S. Zhao, J. Wang, Post-combustion CO2 capture with membrane process: practical membrane performance and appropriate pressure, J. Membr. Sci. 581 (2019) 195–213, https://doi.org/10.1016/j.memsci.2019.03.052.

[2] A.R. Kamble, C.M. Patel, Z.V.P. Murthy, A review on the recent advances in mixed matrix membranes for gas separation processes, Renew. Sustain. Energy Rev. 145 (2021), 111062, https://doi.org/10.1016/j.rser.2021.111062.

[3] K. Friess, P. Izák, M. Kárászová, M. Pasichnyk, M. Lanč, D. Nikolaeva, P. Luis, J. C. Jansen, A review on ionic liquid gas separation membranes, Membranes 11 (2021) 1–58, https://doi.org/10.3390/membranes11020097.

[4] M. Kárászová, B. Zach, Z. Petrusová, V. Červenka, M. Bobák, M. Šyc, P. Izák, Post-combustion carbon capture by membrane separation, Review, Sep. Purif. Technol. 238 (2020) 116448, https://doi.org/10.1016/j.seppur.2019.116448.

[5] M. Klepić, K. Setničková, M. Lanč, M. Žák, P. Izák, M. Dendisová, A. Fuoco, J. C. Jansen, K. Friess, Permeation and sorption properties of CO2-selective blend membranes based on polyvinyl alcohol (PVA) and 1-ethyl-3-methylimidazolium dicyanamide ([EMIM][DCA]) ionic liquid for effective CO2/H2 separation, J. Membr. Sci. 597 (2020) 117623, https://doi.org/10.1016/j.memsci.2019.117623.

[6] M. Galizia, W.S. Chi, Z.P. Smith, T.C. Merkel, R.W. Baker, B.D. Freeman, 50th anniversary perspective: polymers and mixed matrix membranes for gas and vapor separation: a review and prospective opportunities, Macromolecules 50 (2017) 7809–7843, https://doi.org/10.1021/acs.macromol.7b01718.

[7] M.Y. Abdelrahim, C.F. Martins, L.A. Neves, C. Capasso, C.T. Supuran, I. M. Coelhoso, J.G. Crespo, M. Barboiu, Supported ionic liquid membranes immobilized with carbonic anhydrases for CO2 transport at high temperatures, J. Membr. Sci. 528 (2017) 225–230, https://doi.org/10.1016/j.memsci.2017.01.033.

[8] L.A. Neves, J.G. Crespo, I.M. Coelhoso, Gas permeation studies in supported ionic liquid membranes, J. Membr. Sci. 357 (2010) 160–170, https://doi.org/10.1016/j.memsci.2010.04.016.

[9] L.A. Neves, N. Nemestóthy, V.D. Alves, P. Cserjési, K. Bélafi-Bakó, I.M. Coelhoso, Separation of biohydrogen by supported ionic liquid membranes, Desalination 240 (2009) 311–315, https://doi.org/10.1016/j.desal.2007.10.095.

[10] L.C. Tomé, A.S.L. Gouveia, M.A. Ab Ranii, P.D. Lickiss, T. Welton, I.M. Marrucho, Study on gas permeation and CO2 separation through ionic liquid-based membranes with siloxane-functionalized cations, Ind. Eng. Chem. Res. 56 (2017) 2229–2239, https://doi.org/10.1021/acs.iecr.6b04661.

[11] A.R. Nabais, A.P.S. Martins, V.D. Alves, J.G. Crespo, I.M. Marrucho, L.C. Tomé, L. A. Neves, Poly(ionic liquid)-based engineered mixed matrix membranes for CO2/H2 separation, Separ. Purif. Technol. 222 (2019) 168–176, https://doi.org/10.1016/j.seppur.2019.04.018.

[12] L.C. Tomé, D.C. Guerreiro, R.M. Teodoro, V.D. Alves, I.M. Marrucho, Effect of polymer molecular weight on the physical properties and CO2/N2separation of pyrrolidinium-based poly(ionic liquid) membranes, J. Membr. Sci. 549 (2018) 267–274, https://doi.org/10.1016/j.memsci.2017.12.019.

[13] Z.V. Singh, M.G. Cowan, W.M. McDanel, Y. Luo, R. Zhou, D.L. Gin, R.D. Noble, Determination and optimization of factors affecting CO2/CH4separation performance in poly(ionic liquid)-ionic liquid-zeolite mixed-matrix membranes, J. Membr. Sci. 509 (2016) 149–155, https://doi.org/10.1016/j.memsci.2016.02.034.

[14] M.G. Cowan, D.L. Gin, R.D. Noble, Poly(ionic liquid)/ionic liquid ion-gels with high "free" ionic liquid content: platform membrane materials for CO2/light gas separations, Acc. Chem. Res. 49 (2016) 724–732, https://doi.org/10.1021/acs.accounts.5b00547.
[15] K. Friess, J.C. Jansen, F. Bazzarelli, P. Izák, V. Jarmarová, M. Kačírková, J. Schauer, G. Clarizia, P. Bernardo, High ionic liquid content polymeric gel membranes: correlation of membrane structure with gas and vapour transport properties, J. Membr. Sci. 415–416 (2012) 801–809, https://doi.org/10.1016/j.memsci.2012.05.072.
[16] H.R. Mahdavi, N. Azizi, M. Arzani, T. Mohammadi, Improved CO2/CH4 separation using a nanocomposite ionic liquid gel membrane, J. Nat. Gas Sci. Eng. 46 (2017) 275–288, https://doi.org/10.1016/j.jngse.2017.07.024.
[17] M. Klepić, A. Fuoco, M. Monteleone, E. Esposito, K. Friess, Z. Petrusová, P. Izák, J. C. Jansen, Tailoring the thermal and mechanical properties of poly activeTM poly (Ether-Ester) multiblock copolymers via blending with CO2-phylic ionic liquid, Polymers 12 (2020) 890, https://doi.org/10.3390/POLYM12040890.
[18] L. Tomé, C. Liliana, J.E. Porcarelli, M. Bara, D. Forsyth, Mecerreyes, Emerging iongel materials towards applications in energy and bioelectronics, Mater. Horiz. 8 (2021) 3239–3265, https://doi.org/10.1039/D1MH01263K.
[19] A.P.S. Martins, A.F. De Añastro, J.L. Olmedo-Martínez, A.R. Nabais, L.A. Neves, D. Mecerreyes, L.C. Tomé, Influence of anion structure on thermal, mechanical and CO2 solubility properties of uv-cross-linked poly(Ethylene glycol) diacrylate iongels, Membranes 10 (2020) 46, https://doi.org/10.3390/membranes10030046.
[20] M. Li, X. Zhang, S. Zeng, L. Bai, H. Gao, J. Deng, Q. Yang, S. Zhang, Pebax-based composite membranes with high gas transport properties enhanced by ionic liquids for CO2 separation, RSC Adv. 7 (2017) 6422–6431, https://doi.org/10.1039/c6ra27221e.
[21] L. Hao, P. Li, T. Yang, T.S. Chung, Room temperature ionic liquid/ZIF-8 mixed-matrix membranes for natural gas sweetening and post-combustion CO2 capture, J. Membr. Sci. 436 (2013) 221–231, https://doi.org/10.1016/j.memsci.2013.02.034.
[22] Y.C. Hudiono, T.K. Carlisle, J.E. Bara, Y. Zhang, D.L. Gin, R.D. Noble, A three-component mixed-matrix membrane with enhanced CO2separation properties based on zeolites and ionic liquid materials, J. Membr. Sci. 350 (2010) 117–123, https://doi.org/10.1016/j.memsci.2009.12.018.
[23] R. Shindo, M. Kishida, H. Sawa, T. Kidesaki, S. Sato, S. Kanehashi, K. Nagai, Characterization and gas permeation properties of polyimide/ZSM-5 zeolite composite membranes containing ionic liquid, J. Membr. Sci. 454 (2014) 330–338, https://doi.org/10.1016/j.memsci.2013.12.031.
[24] W. Fam, J. Mansouri, H. Li, J. Hou, V. Chen, Gelled graphene oxide-ionic liquid composite membranes with enriched ionic liquid surfaces for improved CO2 separation, ACS Appl. Mater. Interfaces 10 (2018) 7389–7400, https://doi.org/10.1021/acsami.7b18988.
[25] S. Kanehashi, C.A. Scholes, Perspective of mixed matrix membranes for carbon capture, Front. Chem. Sci. Eng. 14 (2020) 460–469, https://doi.org/10.1007/s11705-019-1881-5.
[26] M. Chawla, H. Saulat, M. Masood Khan, M. Mahmood Khan, S. Rafiq, L. Cheng, T. Iqbal, M.I. Rasheed, M.Z. Farooq, M. Saeed, N.M. Ahmad, M.B. Khan Niazi, S. Saqib, F. Jamil, A. Mukhtar, N. Muhammad, Membranes for CO2/CH4 and CO2/N2 gas separation, Chem. Eng. Technol. 43 (2020) 184–199, https://doi.org/10.1002/ceat.201900375.
[27] K.K. Wong, Z.A. Jawad, A review and future prospect of polymer blend mixed matrix membrane for CO2 separation, J. Polym. Res. 26 (2019) 1–13, https://doi.org/10.1007/s10965-019-1978-z.
[28] S.Y. Ding, J. Gao, Q. Wang, Y. Zhang, W.G. Song, C.Y. Su, W. Wang, Construction of covalent organic framework for catalysis: Pd/COF-LZU1 in Suzuki-Miyaura coupling reaction, J. Am. Chem. Soc. 133 (2011) 19816–19822, https://doi.org/10.1021/ja206846p.
[29] L. Stegbauer, K. Schwinghammer, B.V. Lotsch, A hydrazone-based covalent organic framework for photocatalytic hydrogen production, Chem. Sci. 5 (2014) 2789–2793, https://doi.org/10.1039/c4sc00016a.
[30] Q. Fang, S. Gu, J. Zheng, Z. Zhuang, S. Qiu, Y. Yan, 3D microporous base-functionalized covalent organic frameworks for size-selective catalysis, Angew. Chem. 126 (2014) 2922–2926, https://doi.org/10.1002/ange.201310500.
[31] S. Wan, F. Gándara, A. Asano, H. Furukawa, A. Saeki, S.K. Dey, L. Liao, M. W. Ambrogio, Y.Y. Botros, X. Duan, S. Seki, J.F. Stoddart, O.M. Yaghi, Covalent organic frameworks with high charge carrier mobility, Chem. Mater. 23 (2011) 4094–4097, https://doi.org/10.1021/cm201140r.
[32] X.H. Liu, C.Z. Guan, D. Wang, L.J. Wan, Graphene-like single-layered covalent organic frameworks: synthesis strategies and application prospects, Adv. Mater. 26 (2014) 6912–6920, https://doi.org/10.1002/adma.201305317.
[33] M. Dogru, M. Handloser, F. Auras, T. Kunz, D. Medina, A. Hartschuh, P. Knochel, T. Bein, A photoconductive thienothiophene-based covalent organic framework showing charge transfer towards included fullerene, Angew. Chem. 125 (2013) 2992–2996, https://doi.org/10.1002/ange.201208514.
[34] G. Das, B.P. Biswal, S. Kandambeth, V. Venkatesh, G. Kaur, M. Addicoat, T. Heine, S. Verma, R. Banerjee, Chemical sensing in two dimensional porous covalent organic nanosheets, Chem. Sci. 6 (2015) 3931–3939, https://doi.org/10.1039/c5sc00512d.
[35] A. Nagai, X. Chen, X. Feng, X. Ding, Z. Guo, D. Jiang, A squaraine-linked mesoporous covalent organic framework, Angew. Chem. 125 (2013) 3858–3862, https://doi.org/10.1002/ange.201300256.
[36] S. Dalapati, S. Jin, J. Gao, Y. Xu, A. Nagai, D. Jiang, An azine-linked covalent organic framework, J. Am. Chem. Soc. 135 (2013) 17310–17313, https://doi.org/10.1021/ja4103293.
[37] J.T. Yu, Z. Chen, J. Sun, Z.T. Huang, Q.Y. Zheng, Cyclotricatechylene based porous crystalline material: synthesis and applications in gas storage, J. Mater. Chem. 22 (2012) 5369–5373, https://doi.org/10.1039/c2jm15159f.
[38] C.J. Doonan, D.J. Tranchemontagne, T.G. Glover, J.R. Hunt, O.M. Yaghi, Exceptional ammonia uptake by a covalent organic framework, Nat. Chem. 2 (2010) 235–238, https://doi.org/10.1038/nchem.548.
[39] ii S.S. Han, H. Furukawa, O.M. Yaghi, W.A.G. I, 08CovalentOrganic-pub.pdf 105, 2008, pp. 11580–11581.
[40] G. Ma, Heping, Hao Ren, Shuang Meng, Zhuojun Yan, Huanyu Zhao, Fuxing Sun, Zhu, A 3D microporous covalent organic framework with exceedingly high C3H8/CH4 and C2 hydrocarbons/CH4 selectivity, Chem. Commun. 49 (2013) 9773–9775, https://doi.org/10.1039/b000000x.
[41] P. Arab, E. Parrish, T. Islamoğlu, H.M. El-Kaderi, Synthesis and evaluation of porous azo-linked polymers for carbon dioxide capture and separation, J. Mater. Chem. A. 3 (2015) 20586–20594, https://doi.org/10.1039/c5ta04308e.
[42] L. Zou, Y. Sun, S. Che, X. Yang, X. Wang, M. Bosch, Q. Wang, H. Li, M. Smith, S. Yuan, Z. Perry, H.C. Zhou, Porous organic polymers for post-combustion carbon capture, Adv. Mater. 29 (2017) 1–35, https://doi.org/10.1002/adma.201700229.
[43] J. Lu, J. Zhang, Facile synthesis of azo-linked porous organic frameworks via reductive homocoupling for selective CO2 capture, J. Mater. Chem. A. 2 (2014) 13831–13834, https://doi.org/10.1039/c4ta03015j.
[44] Z. Yang, H. Zhang, B. Yu, Y. Zhao, Z. Ma, G. Ji, B. Han, Z. Liu, Azo-functionalized microporous organic polymers: synthesis and applications in CO2 capture and conversion, Chem. Commun. 51 (2015) 11576–11579, https://doi.org/10.1039/c5cc03151f.
[45] R. He, S. Cong, S. Xu, S. Han, H. Guo, Z. Liang, J. Wang, Y. Zhang, CO2-philic mixed matrix membranes based on low-molecular-weight polyethylene glycol and porous organic polymers, J. Membr. Sci. 624 (2021), 119081, https://doi.org/10.1016/j.memsci.2021.119081.
[46] J.X. Zhou, X.S. Luo, X. Liu, Y. Qiao, P. Wang, D. Mecerreyes, N. Bogliotti, S.L. Chen, M.H. Huang, Azo-linked porous organic polymers: robust and time-efficient synthesis: via NaBH4-mediated reductive homocoupling on polynitro monomers and adsorption capacity towards aniline in water, J. Mater. Chem. A. 6 (2018) 5608–5612, https://doi.org/10.1039/c8ta00341f.
[47] F. Chen, G. Tian, L. Shi, S. Qi, D. Wu, Nonvolatile write-once read-many-times memory device based on an aromatic hyperbranched polyimide bearing triphenylamine moieties, RSC Adv. 2 (2012) 12879–12885, https://doi.org/10.1039/c2ra21885b.
[48] A.F.M. El-Mahdy, M.G. Mohamed, T.H. Mansoure, H.H. Yu, T. Chen, S.W. Kuo, Ultrastable tetraphenyl-: P -phenylenediamine-based covalent organic frameworks as platforms for high-performance electrochemical supercapacitors, Chem. Commun. 55 (2019) 14890–14893, https://doi.org/10.1039/c9cc08107k.
[49] H. Bin Zhu, Z.Y. Sun, Aqueous detection of antibiotics with a Cd(II)-based metal-organic framework constructed by a tetra(1,2,4-triazole)-functionalized-bis (triphenylamine) ligand, Inorg. Chem. Commun. 96 (2018) 202–205, https://doi.org/10.1016/j.inoche.2018.08.021.
[50] E.L. Cussler, Fundamentals of Mass Transfer, third ed., Cambridge University Press, New York, 2009 https://doi.org/10.1017/CBO9780511805134.010.
[51] R. Selyanchyn, M. Ariyoshi, S. Fujikawa, Thickness effect on CO 2/N 2 separation in double layer pebax-1657®/PDMS membranes, Membranes 8 (2018), https://doi.org/10.3390/membranes8040121.
[52] J.M.S. Henis, M.K. Tripodi, Composite hollow fiber membranes for gas separation: the resistance model approach, J. Membr. Sci. 8 (1981) 233–246, https://doi.org/10.1016/S0376-7388(00)82312-1.
[53] H.A. Patel, S. Hyun Je, J. Park, D.P. Chen, Y. Jung, C.T. Yavuz, A. Coskun, Unprecedented high-temperature CO2 selectivity in N 2-phobic nanoporous covalent organic polymers, Nat. Commun. 4 (2013) 1–8, https://doi.org/10.1038/ncomms2359.
[54] P.M. Budd, E.S. Elabas, B.S. Ghanem, S. Makhseed, N.B. McKeown, K.J. Msayib, C. E. Tattershall, D. Wang, Solution-processed, organophilic membrane derived from a polymer of intrinsic microporosity, Adv. Mater. 16 (2004) 456–459, https://doi.org/10.1002/adma.200306053.
[55] J. Jeromenok, J. Weber, Solution-processed, organophilic membrane derived from a polymer of intrinsic microporosity, Langmuir 29 (2013) 12982–12989.
[56] H.X. Fu, Z.H. Zhang, W. Fan, S. Wang, Y. Liu, M.H. Huang, A soluble porous organic polymer for highly efficient organic-aqueous biphasic catalysis and convenient reuse of catalysts, J. Mater. Chem. A. 7 (2019) 15048–15053, https://doi.org/10.1039/c9ta04594e.
[57] S.Q. Peng, B. Zhang, W. Fan, S. Wang, Z.H. Zhang, Y. Liu, S.L. Chen, M.H. Huang, Facile synthesis of a porous polynorbornene with an azobenzene subunit: selective adsorption of 4-nitrophenol over 4-aminophenol in water, Polym. Chem. 11 (2020) 6429–6434, https://doi.org/10.1039/d0py00994f.
[58] M. Thommes, K. Kaneko, A.V. Neimark, J.P. Olivier, F. Rodriguez-Reinoso, J. Rouquerol, K.S.W. Sing, Physisorption of gases, with special reference to the evaluation of surface area and pore size distribution (IUPAC Technical Report), Pure Appl. Chem. 87 (2015) 1051–1069, https://doi.org/10.1515/pac-2014-1117.
[59] P. Arab, M.G. Rabbani, A.K. Sekizkardes, T. Islamoğlu, H.M. El-Kaderi, Copper(I)-catalyzed synthesis of nanoporous azo-linked polymers: impact of textural properties on gas storage and selective carbon dioxide capture, Chem. Mater. 26 (2014) 1385–1392, https://doi.org/10.1021/cm403161e.
[60] K. Hosaka, J. Tagami, Y. Nishitani, M. Yoshiyama, M. Carrilho, F.R. Tay, K.A. Agee, D.H. Pashley, Effect of wet vs. dry testing on the mechanical properties of hydrophilic self-etching primer polymers, Eur. J. Oral Sci. 115 (2007) 239–245, https://doi.org/10.1111/j.1600-0722.2007.00452.x.
[61] A. Hassan, N.A. Rahman, R. Yahya, Moisture absorption effect on thermal, dynamic mechanical and mechanical properties of injection-molded short glass-fiber/

polyamide 6,6 composites, Fibers Polym. 13 (2012) 899–906, https://doi.org/10.1007/s12221-012-0899-9.
[62] B.W. Rowe, L.M. Robeson, B.D. Freeman, D.R. Paul, Influence of temperature on the upper bound: theoretical considerations and comparison with experimental results, J. Membr. Sci. 360 (2010) 58–69, https://doi.org/10.1016/j.memsci.2010.04.047.
[63] L.M. Robeson, The upper bound revisited, J. Membr. Sci. 320 (2008) 390–400, https://doi.org/10.1016/j.memsci.2008.04.030.
[64] E. Kamio, T. Yasui, Y. Iida, J.P. Gong, H. Matsuyama, Inorganic/organic double-network gels containing ionic liquids, Adv. Mater. 29 (2017) 1–8, https://doi.org/10.1002/adma.201704118.
[65] F. Ranjbaran, E. Kamio, H. Matsuyama, Ion gel membrane with tunable inorganic/organic composite network for CO2 separation, Ind. Eng. Chem. Res. 56 (2017) 12763–12772, https://doi.org/10.1021/acs.iecr.7b03279.
[66] A.R. Nabais, R.P.P.L. Ribeiro, J.P.B. Mota, V.D. Alves, I.A.A.C. Esteves, L.A. Neves, CO2/N2 gas separation using Fe(BTC)-based mixed matrix membranes: a view on the adsorptive and filler properties of metal-organic frameworks, Separ. Purif. Technol. 202 (2018) 174–184, https://doi.org/10.1016/j.seppur.2018.03.028.
[67] A.M. Sampaio, A.R. Nabais, L.C. Tomé, L.A. Neves, Impact of MOF-5 on pyrrolidinium-based poly(ionic liquid)/ionic liquid membranes for biogas upgrading, Ind. Eng. Chem. Res. 59 (2020) 308–317, https://doi.org/10.1021/acs.iecr.9b04206.